Research Article

Sumera Dero, Abdul Rehman Nangraj, Liaquat Ali Lund, Umair Khan*, and Samia Elattar

Mathematical investigation of Fe_3O_4–Cu/blood hybrid nanofluid flow in stenotic arteries with magnetic and thermal interactions: Duality and stability analysis

https://doi.org/10.1515/htmp-2025-0091
received January 19, 2025; accepted July 15, 2025

Abstract: The present study has potential applications in biomedical engineering, particularly in drug delivery systems and diagnostic imaging of stenotic arteries. The purpose of this study is to explore the key role of Fe_3O_4 and Cu nanoparticles, which are submerged together in human blood in the presence of magnetohydrodynamics flow through stenotic arteries. The main motive for selecting Fe_3O_4 and Cu nanoparticles is their importance in drug delivery because they possess potential usefulness in drug transference as well as imaging properties. Therefore, the governing equations that define the flow as well as heat transference of blood are changed from partial differential equations to ordinary differential equations by utilizing the appropriate similarity variables. The shooting technique was applied to achieve the numerical solution in Maple software to observe the influences of the used nanoparticles and the parameters in stenotic arteries. Velocity and temperature profiles, along with engineering interest quantities, skin friction, and Nusselt numbers, were detected for various values of parameters and nanoparticle volume fractions. The main findings show that dual solutions exist for $S \geq 1.7591$, $\lambda \geq -0.82435$, and $0 \leq \chi \leq 0.7385$. Moreover, the blood flow performance can be decreased by increasing the suction and magnetic parameters and the rate of shrinking in the stenotic arteries. The temperature of the blood can be raised by increasing the rate of thermal radiation and magnetic parameters. An increase in the thermal slip parameter decreased the temperature of the blood in the arteries. Such modeling and investigation of solutions can play an important role in predicting the reasons for atherosclerosis.

Keywords: human blood, nanofluid, shooting method, thermal radiation, magnetic field

*** Corresponding author: Umair Khan**, Department of Mathematics, Saveetha School of Engineering, Saveetha Institute of Medical and Technical Sciences, Saveetha University, Chennai, 602105, Tamil Nadu, India; Department of Mathematics, Faculty of Science, Sakarya University, Serdivan/Sakarya, 54050, Turkey, e-mail: umairkhan@sakarya.edu.tr
Sumera Dero: Institute of Mathematics and Computer Science, University of Sindh, Jamshoro Sindh, 76080, Pakistan, e-mail: sumera.dero@usindh.edu.pk
Abdul Rehman Nangraj: Institute of Mathematics and Computer Science, University of Sindh, Jamshoro Sindh, 76080, Pakistan, e-mail: rehman.nangraj@usindh.edu.pk
Liaquat Ali Lund: KCAMS Khairpur Mir's, Sindh Agriculture University, Tandojam Sindh, 70060, Pakistan, e-mail: balochliaqatali@gmail.com
Samia Elattar: Department of Industrial and Systems Engineering, College of Engineering, Princess Nourah bint Abdulrahman University, P.O. Box 84428, Riyadh 11671, Saudi Arabia, e-mail: SAElattar@pnu.edu.sa

Nomenclature

u_0	Velocity constant
$R(x)$	Radius
u, v	Velocity components
$L_0/2$	Length of the stenotic artery
Cu	Copper
T	Temperature
T_∞	Ambient temperature
T_0	Constant reference temperature
T_w	Wall surface temperature
χ	Flow parameter
k_{hnf}	Thermal conductivity
ϑ	Kinematic viscosity
Re_x	Reynolds number
η	Transformed variable
k^*	Absorption coefficient
γ	Unknown eigenvalue
$B(x)$	Magnetic field
Rd	Thermal radiation
M	Hartmann number

Pr	Prandtl number
δ_{T}	Thermal slip parameter
v_w	Suction/injection velocity
μ_{hnf}	Dynamic viscosity
ρ_{hnf}	Density
$(\rho c_{\mathrm{p}})_{\mathrm{hnf}}$	Heat capacity
Λ	Stretching/shrinking parameter
S	Injection/suction parameter
Nu	Local Nusselt number
C_{f}	Skin friction coefficient
k	Thermal conductivity
Ψ	Stream function
Re_x	Local Reynolds number

1 Introduction

Nanofluids are prepared using the suspension of nanosized materials in traditional fluids. Such fluids exhibit a considerable increase in thermal properties at low nanoparticle concentrations. They exhibit several motivating properties, and their unique structures offer extraordinary potential for modern applications. It is seen that most of the nanofluid publications are about understanding their behavior and characteristics so that they can be used where direct improvement of nanofluids may dominate in different applications of industries, biomedicine, nuclear, transportation, electronics, reactors, and food. The present work mainly concentrates on a wide range of related biological applications that particularly involve nanofluids. Different nanomaterials used in different nanofluids are the main resources in nanotechnology. The smallest range of nanoparticles is particularly used in medical applications, including the treatment of blood vessels. Such fluids can be used for the transportation of medications. Several researchers [1–3] have used different types of nanoparticles to investigate the changing aspects of blood due to stenosed arteries. Atherosclerotic plaques or thinning of the human arterial system, predictable as arterial stenosis, is relatively common. Stenosis disrupts the natural arterial flow pattern of blood. The human kidneys require sufficient blood flow to assist in cleaning useless materials.

Due to arterial constrictions, a typical quantity of oxygen-rich blood cannot reach the human kidneys, which increases blood pressure and causes many injuries. In this regard, Abdelsalam et al. [4] analyzed blood flow through damaged arteries using the osmotic pressure forces of hybrid nanoparticles. The blood flow of hybridized nanofluids through arteries for the respiratory circulatory system and medication administration was studied by Shojaie Chahregh and Dinarvand [5]. While Shahzadi and Bilal [6] considered the impact of permeability on the hybridized flow of blood through the bifurcation of stenotic arteries, a drug transporter application was exposed by Dinarvand et al. [7], who showed that the single shape of the flow of blood of the nanofluids on a stretching surface may improve the treatment of microcirculatory systems. Shivalila et al. [8] investigated the role of thermophoretic particle deposition effects in a blood nanofluid flow past a stenosed artery with porous medium. Zhang et al. [9] analyzed the effect of a soft magnetic particle content on the multiphysics field of a magnetorheological composite gel clutch with a complex flow channel excited by a Halbach array arrangement. Saeed et al. [10] investigated the flow of the blood-based hybridized nanofluid in the presence of the couple stress and electromagnetic field. The flow of nanofluids along the radiation effect over vertically damaged coronary arteries was studied by Kot and Elmaboud [11]. The Casson base hybrid nanofluid flow with up and down tawdriness in thinner films was investigated by Alhussain and Tassaddiq [12]. Moreover, Sajid et al. [13] studied the influence of oxic organisms as well as the diffusivity of diverse species on gold blood relations. Mousavi et al. [14] inspected the magnetohydrodynamic flow of the heat radiative hybrid nanofluids with dual solutions over the spinning thinner spine. Parveen et al. [15] studied the energy transference and stress increase of hybrid nanofluids with magnetic fields and endoscopic effects induced using a computational technique.

Nanofluids are ultra-fine nanomaterial suspensions in conventional fluids. The main reason for developing nanofluids was to enhance the thermal conductivities in the flows of fluids that have been extensively validated for thermal manufacturing and technical usage, similar to computer disc drives, coolants in vehicles, turbojet engines, and chemical operations. The nanofluid was first introduced by American scientists Choi and Eastman [16], who made it an active field of research. Scientists and researchers have emphasized the outstanding heat transfer proficiencies of nanofluids in the literature. Farooq et al. [17] investigated the flow of the bio-convective Carreau blood-based hybridized nanofluids with Cattaneo Christov mass and heat exchange. Li et al. [18] studied the second-grade nanofluid flow with Wu's slip and motile microorganisms. Nanotechnology is a comprehensive scientific research discipline. Therefore, the development of nanostructures in medicine and drug distribution in the body is mainly related to creating an artificial nanometer-sized tailored delivery system for medication. Microcapsules, liposomes, microparticles, nanoemulsions, and many other drug-delivery methods exhibit a wider range of useful properties. They have numerous advantages and disadvantages. Each system was developed to

address the shortcomings of previously used systems. In this regard, Motasadizadeh et al. [19] examined a twin medication-delivering hydrogel scaffold based on sodium alginate for the treatment of chronic bone infections. Sabzi et al. [20] studied the corrosion responses and bioactivity of ZnO nanoparticles placed on an NiTi shape memory alloy. The surface narrative of nanocomposites along CuO for the visible-light antimicrobial applications and photocatalytic antibiotic degradation was investigated by Hajipour et al. [21]. In this regard, some important studies have been conducted [22–26].

This study aimed to investigate the importance of Fe_3O_4–Cu/blood base hybrid nanofluids through stenosed arteries. In this study, stretching/shrinking cases of porous media were discussed. The effects of magnetic, suction, radiation, thermal slip, and the combined effects of Fe_3O_4 and Cu were examined. To the best of our knowledge, such an innovative study has not been reported in the literature. The governing partial differential equations (PDEs) are converted into ordinary differential equations (ODEs) using appropriate similarity transformations. Then, the equations are solved numerically by applying the shooting technique in Maple software. The results were validated by comparing the results obtained in this study with those previously reported in the literature. Parameter duality in solutions is obtained at different ranges. This study leads us toward fruitful applications of nanofluids in medicine. However, there is a need to work in this field on theoretical and experimental bases, considering different types of nanoparticles and physical parameters.

2 Mathematical formulation

Let us consider the steady 2D MHD laminar, incompressible, and heat transfer behavior of a Fe_3O_4–Cu/blood hybrid nanofluid flow, along with the thermal radiation effect through a stenosed artery. The following key assumptions have been made:

- **Flow Parameters:** Various factors influencing the flow are considered, such as thermal radiation effects, magnetic forces, thermal slip, and suction.
- **Stenosis Geometry**: The stenosed artery has a total length of $L_0/2$. The radius of the artery is represented by $R(x)$, with stenosis characterized by a height χ and a width in the unrestricted region of $(2R_0)$.
- **Coordinate System**: The coordinate system is chosen such that the blood flow moves along the x-axis and perpendicular to the r-axis.

Figure 1 illustrates the flow pattern and coordinate system used in the model. The profile of the stenosed region was based on the work of Sarwar et al. [27].

$$\begin{cases} R(x) = -\frac{1}{2}\left\{1 + \cos\left(\frac{4\pi x}{L_0}\right)\right\}\chi + R_0, & -\frac{L_0}{4} < x < \frac{L_0}{4} \\ R(x) = R_0 \quad \text{otherwise.} \end{cases} \tag{1}$$

Based on the above assumptions and boundary layer approximations or scaling, the following leading equations of the considered problem are given as follows [27]:

$$\frac{\partial(rv)}{\partial r} + \frac{\partial(ru)}{\partial x} = 0, \tag{2}$$

$$\rho_{\text{hnf}}\left(v\frac{\partial u}{\partial r} + u\frac{\partial u}{\partial x}\right) = -\sigma_{\text{hnf}}B_0^2 u + \mu_{\text{hnf}}\frac{\partial(ru_r)}{r\partial r}, \tag{3}$$

$$(\rho c_{\text{p}})_{\text{hnf}}\left(v\frac{\partial T}{\partial r} + u\frac{\partial T}{\partial x}\right) = k_{\text{hnf}}\frac{1}{r}\frac{\partial(rT_r)}{\partial r} - \frac{1}{r}\frac{\partial(rq_r)}{\partial r}, \tag{4}$$

where q_r is the radiation heat exchange and can be defined as

$$q_r = -\frac{4\sigma^*}{3k^*}\frac{\partial T^4}{\partial r}, \tag{5}$$

where k^* is the mean absorption coefficient and σ^* is the Stefan–Boltzmann constant. The temperature variance in the flow is considered to be adequately smaller; therefore, T^4 is defined as the linear relation of temperature T and using truncated Taylor's series on the free-stream flowing fluid temperature T_∞ and later, ignoring greater order terms, there would be:

$$T^4 \cong -3T_\infty^4 + 4T_\infty^3 T. \tag{6}$$

Using equation (6) in equation (4), we obtain

$$(\rho c_{\text{p}})_{\text{hnf}}\left(u\frac{\partial T}{\partial x} + v\frac{\partial T}{\partial r}\right) = k_{\text{hnf}}\frac{\partial(rT_r)}{r\partial r} + \frac{16\sigma^* T_\infty^3}{3k^*}\frac{\partial T_r}{\partial r}. \tag{7}$$

The boundary conditions considered are as follows:

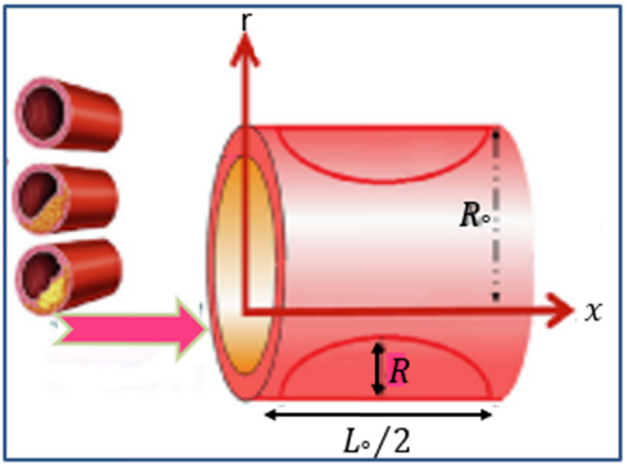

Figure 1: Physical sketch of the flow model and the cylindrical coordinate system.

$$u = \lambda u_w, \quad v = v_w, \quad T = T_w + N\frac{\partial T}{\partial r} \text{ at } r = R, \\ u \to 0, \quad T \to T_\infty, \quad \text{as } R \to \infty, \tag{8}$$

where u and v correspond to the velocity components in the directions of the x- and r-axis, respectively. σ_f is the electrical conduction,T is the temperature of the hybrid nanofluid, ρ_{hnf} is the density of HNFs, μ_{hnf} is the viscosity of the HNFs, $(\rho C_{\text{p}})_{\text{hnf}}$ is the heat capacity of HNFs, and k_{hnf} is the thermal conductivity of the HNFs that are further defined in Table 1. Moreover, the stretching and shrinking parameters is denoted by λ, where $\lambda < 0$ and $\lambda > 0$ show the shrinking and stretching cases of arterial surfaces, respectively.

Continuity equation (1) is satisfied by presenting ψ as the stream function for the velocity components u and v defined as

$$u = \frac{\partial \psi}{r\partial r}, \; v = -\frac{\partial \psi}{r\partial x}, \tag{9}$$

where $\psi = \sqrt{\frac{\upsilon_{\text{f}} u_0}{L_0}}\, xRf(\eta)$.

Using equation (9) in equations (3) and (7), we obtain

$$\rho_{\text{hnf}}\left(\frac{1}{r}\frac{\partial \psi}{\partial r}\frac{\partial}{\partial x}\left(\frac{1}{r}\frac{\partial \psi}{\partial r}\right) - \frac{1}{r}\frac{\partial \psi}{\partial x}\frac{\partial}{\partial r}\left(\frac{1}{r}\frac{\partial \psi}{\partial x}\right)\right) \\ = \mu_{\text{hnf}}\frac{1}{r}\frac{\partial}{\partial r}\left(\frac{\partial^2 \psi}{\partial r^2} - \frac{1}{r}\frac{\partial \psi}{\partial r}\right) - \sigma_{\text{hnf}} B_0^2\left(\frac{1}{r}\frac{\partial \psi}{\partial r}\right), \tag{10}$$

$$(\rho c_{\text{p}})_{\text{hnf}}\left(\frac{1}{r}\frac{\partial \psi}{\partial r}\frac{\partial T}{\partial x} - \frac{1}{r}\frac{\partial \psi}{\partial x}\frac{\partial T}{\partial r}\right) \\ = k_{\text{hnf}}\frac{1}{r}\frac{\partial (rT_r)}{\partial r} + \frac{16\sigma^* T_\infty^3}{3k^*}\frac{\partial T_r}{\partial r}. \tag{11}$$

To detect similarity solutions of equations (10) and (11), the following similarity transformation is considered:

$$u = \frac{u_0 x}{L_0} f(\eta), \; v = \frac{R}{r}\sqrt{\frac{u_0 \upsilon_{\text{f}}}{L_0}}\, f(\eta), \\ \eta = \frac{r^2 - R^2}{2R}\sqrt{\frac{u_0}{\upsilon_{\text{f}} L_0}}, \quad \theta(\eta) = (T - T_\infty)/(T_{\text{f}} - T_\infty), \tag{12}$$

which is obtained using similarity variables (12) in equations (10) and (11). Thus,

$$\frac{\mu_{\text{hnf}}/\mu_{\text{f}}}{\rho_{\text{hnf}}/\rho_{\text{f}}}[(1 + 2\eta\chi)f'''(\eta) + 2\chi f''(\eta)] \\ + f(\eta)f''(\eta) - \left(\frac{\sigma_{\text{hnf}}}{\sigma_{\text{f}}}M + f'(\eta)\right)f'(\eta) = 0, \tag{13}$$

$$\frac{1}{\Pr(\rho c_{\text{p}})_{\text{hnf}}/(\rho c_{\text{p}})_{\text{f}}}\left(\frac{k_{\text{hnf}}}{k_{\text{f}}} + \frac{4}{3}\text{Rd}\right) \\ \times [(1 + 2\eta\chi)\theta''(\eta) + 2\chi\theta'(\eta)] + \theta'(\eta)f(\eta) = 0, \tag{14}$$

with the following boundary conditions:

$$f'(0) = \lambda, \quad f(0) = S, \quad \theta(0) = 1 + \delta_T\theta'(0) \\ f'(\eta) \to 0, \quad \theta(\eta) \to 0 \text{ as } \eta \to \infty. \tag{15}$$

The dimensionless flow parameters are defined as

$M = \frac{L_0\sigma_{\text{f}}B_0^2}{\rho_{\text{f}}u_0}$	Magnetic parameter
$S = -v_w\frac{r}{R}\sqrt{\frac{L_0}{\upsilon_{\text{f}}u_0}}$	Injection parameter
$\chi = \sqrt{\frac{\upsilon_{\text{f}}L_0}{R^2u_0}}$	Flow parameter
$\text{Rd} = \frac{4\sigma^* T_\infty^3}{k_{\text{f}}k^*}$	Radiation parameter
$\delta_{\text{T}} = \left(\frac{u_0}{\upsilon_{\text{f}}L_0}\right)^{1/2} N$	Thermal slip parameter
$\Pr = \frac{k_{\text{f}}}{(\mu C_{\text{p}})_{\text{f}}}$	Prandtl number

3 Quantities of engineering interest

The quantities of engineering interest, skin friction (C_{f_x}), and local Nusselt number (Nu_x) are defined as

$$C_{f_x} = \frac{2\tau_w}{U_w^2\rho_{\text{f}}} \text{ and } \text{Nu}_x = \frac{xq_w}{k_{\text{f}}(T_w - T_\infty)}, \tag{16}$$

Table 1: Correlation of the thermophysical properties between the base fluid and nanoparticles according to Sharma et al. [28]

Property	Mathematical formulations of hybrid nanofluids
Density	$\rho_{\text{hnf}} = [(1 - \varphi_{Fe_3O_4})\rho_{\text{f}} + \varphi_{Fe_3O_4}\rho_{Fe_3O_4}](1 - \varphi_{\text{Cu}}) + \varphi_{\text{Cu}}\rho_{\text{Cu}}$
Dynamic viscosity	$\mu_{\text{hnf}} = \mu_{\text{f}}(1 - \varphi_{\text{Cu}})^{-2.5}(1 - \varphi_{Fe_3O_4})^{-2.5}$
Heat capacity	$(\rho c_{\text{p}})_{\text{hnf}} = [(1 - \varphi_{Fe_3O_4})(\rho c_{\text{p}})_{\text{f}} + \varphi_{Fe_3O_4}(\rho c_{\text{p}})_{Fe_3O_4}](1 - \varphi_{\text{Cu}}) + \varphi_{\text{Cu}}(\rho c_{\text{p}})_{\text{Cu}}$
Thermal conductivity	$k_{\text{hnf}} = \frac{2k_{\text{nf}} + k_{\text{Cu}} - 2\varphi_{\text{Cu}}(k_{\text{nf}} - k_{\text{Cu}})}{2k_{\text{nf}} + k_{\text{Cu}} + \varphi_{\text{Cu}}(k_{\text{nf}} - k_{\text{Cu}})} \times (k_{\text{nf}})$, where $k_{\text{nf}} = \frac{2k_{\text{f}} - 2\varphi_{Fe_3O_4}(k_{\text{f}} - k_{Fe_3O_4}) + k_{Fe_3O_4}}{2k_{\text{f}} + \varphi_{Fe_3O_4}(k_{\text{f}} - k_{Fe_3O_4}) + k_{Fe_3O_4}} \times (k_{\text{f}})$
Electrical conductivity	$\sigma_{\text{hnf}} = \frac{\sigma_{\text{Cu}} + 2\sigma_{\text{nf}} - 2\phi_{\text{Cu}}(\sigma_{\text{nf}} - \sigma_{\text{Cu}})}{\sigma_{\text{Cu}} + 2\sigma_{\text{nf}} + \phi_{\text{Cu}}(\sigma_{\text{nf}} - \sigma_{\text{Cu}})} \times (\sigma_{\text{nf}})$, where $\sigma_{\text{nf}} = \frac{\sigma_{Fe_3O_4} + 2\sigma_{\text{f}} - 2\phi_{Fe_3O_4}(\sigma_{\text{f}} - \sigma_{Fe_3O_4})}{\sigma_{Fe_3O_4} + 2\sigma_{\text{f}} + \phi_{Fe_3O_4}(\sigma_{\text{f}} - \sigma_{Fe_3O_4})} \times (\sigma_{\text{f}})$

where heat flux and shear stress are written as

$$q_w = -k_{\text{hnf}} T_r|_{r=R} + q_{\text{rad}}|_{r=R} \text{ and}$$
$$\tau_w = \mu_{\text{hnf}} u_r|_{r=R}. \tag{17}$$

Using equations (12) and (17) in equation (16), we obtain

$$\sqrt{\text{Re}_x} C_{f_x} = \frac{\mu_{\text{hnf}}}{\mu_{\text{f}}} f''(0) \text{ and}$$
$$\text{Nu}_x/\sqrt{\text{Re}_x} = -\left(\frac{k_{\text{hnf}}}{k_{\text{f}}} + \frac{4}{3}\text{Rd}\right)\theta'(0). \tag{18}$$

3.1 Numerical procedure of the scheme

To obtain the numerical solutions of equations (13) and (14) with boundary conditions (15), the shooting technique in Maple software is applied. Generally, this method converts boundary value problems into related initial value problems. Moreover, this method is very fast in providing numerical results with good convergence and attractive graphical visualizations. According to this methodology, the equations are written as

$$f' = F_{\text{P}}, \quad f'' = F_{\text{PP}},$$
$$\frac{\mu_{\text{hnf}}/\mu_{\text{f}}}{\rho_{\text{hnf}}/\rho_{\text{f}}}[(1 + 2\eta\chi)F'_{\text{PP}} + 2\chi F_{\text{PP}}] - \frac{\sigma_{\text{hnf}}}{\sigma_{\text{f}}} M F_{\text{P}} + F F_{\text{PP}} - (F_{\text{PP}})^2 = 0, \tag{19}$$
$$\theta' = \theta_{\text{P}},$$
$$\frac{1}{\text{Pr}(\rho c_{\text{p}})_{\text{hnf}}/(\rho c_{\text{p}})_{\text{f}}}\left(\frac{k_{\text{hnf}}}{k_{\text{f}}} + \frac{4}{3}\text{Rd}\right)[(1 + 2\eta\chi)\theta'_{\text{P}} + 2\chi\theta_{\text{P}}] + F\theta_{\text{P}} - F_{\text{P}}\theta = 0, \tag{20}$$

with the following boundary conditions:

$$F_{\text{P}}(0) = \lambda, \quad F(0) = S, \quad \theta(0) = 1 + \delta_{\text{T}}\theta_{\text{P}}(0),$$
$$F_{\text{P}}(\eta) \to 0, \quad \theta(\eta) \to 0 \text{ as } \eta \to \infty, \tag{21}$$

where the values of the missing conditions should be carefully considered, as they might satisfy the specified boundary conditions. The results are obtained using shooting methods by aiding the shootlib functions in Maple software. The convergence of all graphs is fixed at blt = 12 for both achieved solutions.

3.2 Stability analysis

Because of the occurrence of dual solutions for each value of the flow parameters, a stability analysis is performed to check their accuracy. In this regard, the unsteady forms of equations (3) and (4) are considered as follows:

$$\frac{\partial u}{\partial t} + v\frac{\partial u}{\partial r} + u\frac{\partial u}{\partial x} = \frac{\mu_{\text{hnf}}}{\rho_{\text{hnf}}}\frac{\partial(ru_r)}{r\partial r} - \frac{\sigma_{\text{hnf}}}{\rho_{\text{hnf}}}B_0^2 u, \tag{22}$$

$$\frac{\partial T}{\partial t} + v\frac{\partial T}{\partial r} + u\frac{\partial T}{\partial x} = \frac{k_{\text{hnf}}}{(\rho c_{\text{p}})_{\text{hnf}}}\frac{1}{r}\frac{\partial(rT_r)}{r\partial r} + \frac{16\sigma^* T_\infty^3}{3(\rho c_{\text{p}})_{\text{hnf}} k^*}\frac{\partial T_r}{\partial r}. \tag{23}$$

Introducing a new time-dependent variable τ and modifying the transformations given in equation (5) for unsteady flow, we obtain

$$\eta = \frac{r^2 - R^2}{2R}\sqrt{\frac{u_0}{\upsilon_f L_0}}, \quad \psi = \sqrt{\frac{\upsilon_f u_0}{L_0}}\, xRf(\eta, \tau)$$
$$\theta(\eta, \tau) = \frac{T - T_\infty}{T_{\text{w}} - T_\infty} \text{ and } \tau = \frac{u_0}{L_0}t, \tag{24}$$

where $u = \frac{u_0 x}{L_0} f(\eta, \tau)$ and $v = -\frac{R}{r}\sqrt{\frac{u_0 \upsilon_f}{L_0}}\, f(\eta, \tau)$.

Thus, using equation (24) in equations (22) and (23), we obtain

$$\frac{\mu_{\text{hnf}}/\mu_{\text{f}}}{\rho_{\text{hnf}}/\rho_{\text{f}}}\left\{(1 + 2\chi\eta)\frac{\partial^3 f(\eta, \tau)}{\partial\eta^3} + 2\chi\frac{\partial^2 f(\eta, \tau)}{\partial\eta^2}\right\} + f(\eta, \tau)\frac{\partial^2 f(\eta, \tau)}{\partial\eta^2} - \left\{\frac{\partial f(\eta, \tau)}{\partial\eta}\right\}^2 - \frac{\sigma_{\text{hnf}}}{\sigma_{\text{f}}}M\frac{\partial f(\eta, \tau)}{\partial\eta} - \frac{\partial^2 f(\eta, \tau)}{\partial\eta\partial\tau} = 0, \tag{25}$$

$$\frac{1}{\text{Pr}(\rho c_{\text{p}})_{\text{hnf}}/(\rho c_{\text{p}})_{\text{f}}}\left(\frac{k_{\text{hnf}}}{k_{\text{f}}} + \frac{4\text{Rd}}{3}\right) \times \left[2\chi\frac{\partial\theta(\eta, \tau)}{\partial\eta} + (1 + 2\eta\chi)\frac{\partial^2\theta(\eta, \tau)}{\partial\eta^2}\right] + \frac{\partial\theta(\eta, \tau)}{\partial\eta}f(\eta, \tau) - \frac{\partial\theta(\eta, \tau)}{\partial\tau} = 0, \tag{26}$$

with the following boundary conditions:

$$\begin{cases} \dfrac{\partial f(0, \tau)}{\partial\eta} = \lambda, \quad f(0, \tau) = S, \quad \theta(0, \tau) - 1 = \delta_{\text{T}}\dfrac{\partial\theta(0, \tau)}{\partial\eta} \\ \dfrac{\partial f(\eta, \tau)}{\partial\eta} \to 0, \quad \theta(\eta, \tau) \to 0 \text{ as } \eta \to \infty. \end{cases} \tag{27}$$

The perturbed basic solutions $f(\eta) = f_0(\eta)$ and $\theta(\eta) = \theta_0(\eta)$ with disturbances are expressed as

$$\begin{cases} f(\eta, \tau) = \text{e}^{-\gamma\tau}F(\eta, \tau) + f_0(\eta) \\ \theta(\eta, \tau) = \text{e}^{-\gamma\tau}G(\eta, \tau) + \theta_0(\eta), \end{cases} \tag{28}$$

where γ is the smallest eigenvalue and both $F(\eta, \tau)$ and $G(\eta, \tau)$ are the smallest relative to $f_0(\eta)$ and $\theta_0(\eta)$, respectively. Using equation (28) in equations (25) and (27), a

Table 2: Thermophysical properties of blood with Cu and Fe_3O_4 nanomaterials as given by Mutuku-Njane [30]

	ρ (kg · m^{-3})	C_p (kg · k^{-1})	k (W·m^{-1} · k^{-1})	σ(s·m^{-1})
Blood	1,063	3,594	0.492	6.67×10^{-1}
Cu	8,933	385	401	5.96×10^{7}
Fe_3O_4	5,180	670	80.4	1.12×10^{5}

linear eigenvalue problem is obtained.

$$\frac{\mu_{hnf}/\mu_f}{\rho_{hnf}/\rho_f}\left\{(1+2\chi\eta)\frac{\partial^3 F}{\partial\eta^3}+2\chi\frac{\partial^2 F}{\partial\eta^2}\right\}+Ff_0''+f_0\frac{\partial^2 F}{\partial\eta^2}-2f_0'\frac{\partial F}{\partial\eta}-\frac{\sigma_{hnf}}{\sigma_f}M\frac{\partial F}{\partial\eta}+\gamma\frac{\partial F}{\partial\eta}-\frac{\partial^2 F}{\partial\eta\partial\tau}=0, \tag{29}$$

$$\frac{1}{\Pr(\rho c_p)_{hnf}/(\rho c_p)_f}\left(\frac{k_{hnf}}{k_f}+\frac{4\mathrm{Rd}}{3}\right)\left[2\chi\frac{\partial G}{\partial\eta}+(1+2\eta\chi)\frac{\partial^2 G}{\partial\eta^2}\right]+f_0\frac{\partial G}{\partial\eta}+F\theta_0'+\gamma G-\frac{\partial G}{\partial\tau}=0, \tag{30}$$

with the following boundary conditions:

$$\begin{cases}\dfrac{\partial F}{\partial\eta}=0,\quad F(0,\tau)=0,\quad G(0,\tau)=0,\\ \dfrac{\partial F}{\partial\eta}\to 0,\quad G(\eta,\tau)\to 0\ \text{as}\ \eta\to\infty.\end{cases} \tag{31}$$

The solutions $f(\eta) = f_0(\eta)$ and $\theta(\eta) = \theta_0(\eta)$ of the steady equations (13) and (14) are obtained by considering $\tau = 0$. Therefore, $F(\eta) = F_0(\eta)$ and $G(\eta) = G_0(\eta)$ in equations (29) and (30) detect the initial decay or growth of solutions. Ultimately, it is achieved as follows:

$$\frac{\mu_{hnf}/\mu_f}{\rho_{hnf}/\rho_f}\{(1+2\chi\eta)F_0''+2\chi F_0'\}+F_0f_0''+f_0F_0''-2f_0'F_0'-\frac{\sigma_{hnf}}{\sigma_f}MF_0'+\gamma F_0'=0, \tag{32}$$

$$\frac{1}{\Pr(\rho c_p)_{hnf}/(\rho c_p)_f}\left(\frac{k_{hnf}}{k_f}+\frac{4\mathrm{Rd}}{3}\right)[2\chi G_0'+(1+2\eta\chi)G_0'']+f_0G_0'+F_0\theta_0'+\gamma G_0=0, \tag{33}$$

Table 3: Comparative results of the temperature gradient $-\theta''(0)$ for various values of the other parameters used at $\mathrm{Rd} = M = \delta_T = \varphi_{hnf} = 0$

Pr	λ	χ	Rangi and Ahmad [31]	Present study
1	1	0.0	−0.985286	−0.985290
		0.25	−1.079447	−1.079448
		0.5	−1.173899	−1.173908

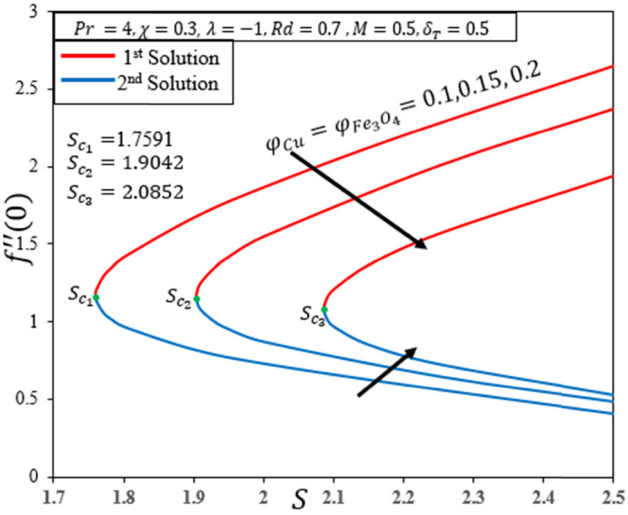

Figure 2: Variations in $f''(0)$ along S for various Fe_2O_4 and Cu nanoparticles.

with the following boundary conditions:

$$\begin{cases}F_0(0)=0,\quad F_0'(0)=0,\quad G_0(0)=0,\\ F_0'(\eta)\to 0,\quad G_0(\eta)\to 0,\quad \text{as}\ \eta\to\infty.\end{cases} \tag{34}$$

The stability analysis of equations (32) and (33), with boundary conditions (34), was performed for variations in λ and S to achieve the smallest related eigenvalues γ using bvp4c in MATLAB, as proposed by Harris et al. [29]. Moreover, a series of possible eigenvalues can be achieved by relaxing one of the boundary conditions on $F_0(\eta)$ or $G_0(\eta)$. In this problem, $F_0'(\eta)\to 0$ is relaxed as $\eta\to\infty$ as $F_0''(\eta) = 1$.

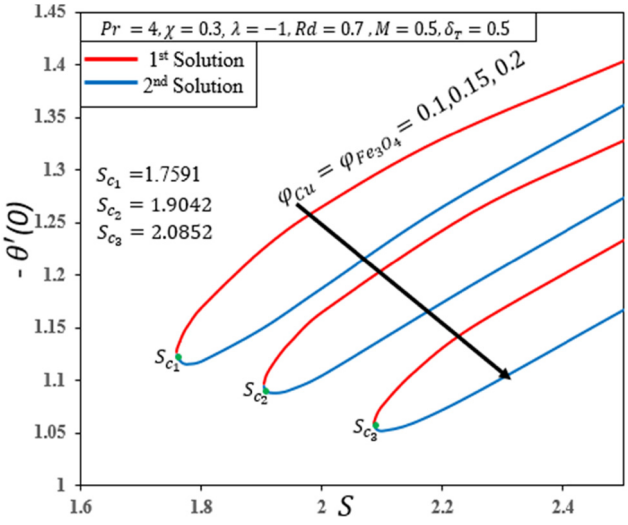

Figure 3: Variations in $\theta'(0)$ along S for various Fe_3O_4 and Cu nanoparticles.

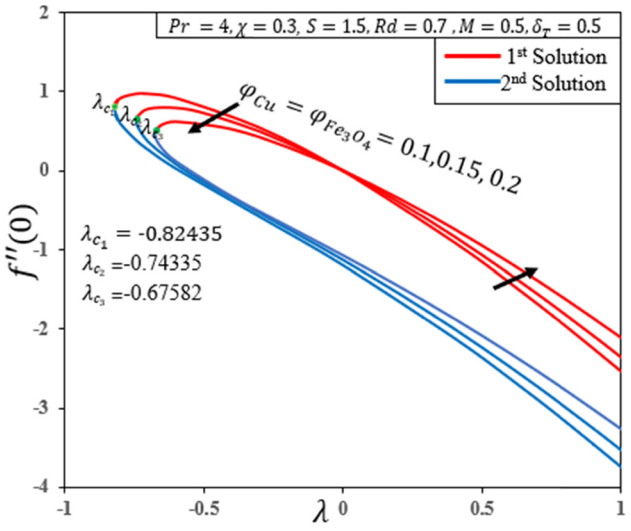

Figure 4: Variations in $f''(0)$ along λ for various Fe_3O_4 and Cu nanoparticles.

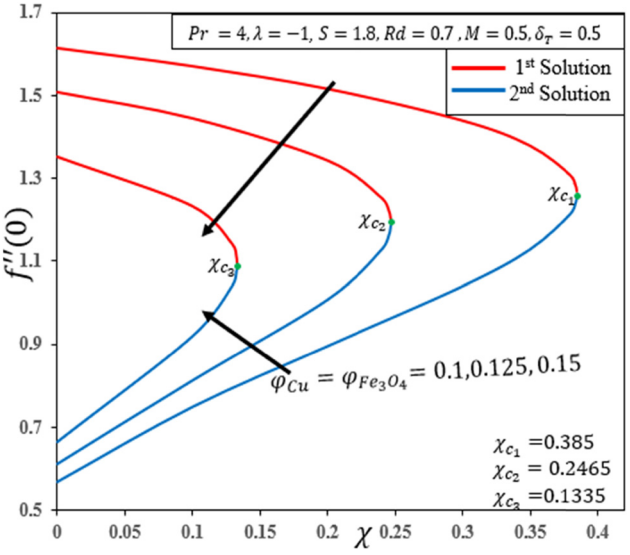

Figure 6: Variations in $f''(0)$ along χ for various Fe_3O_4 and Cu nanoparticles.

4 Results and discussion

The system of non-linear equations (13) and (14), which follow the boundary conditions (15), was numerically solved using the shooting technique through Maple software to examine the influences of specified nanomaterials and various flow parameters in human blood flow that is affected by the stenotic artery. The numerical values of the thermophysical properties of different nanomaterials used and base fluids are presented in Table 2. Owing to the duality in solutions, the stability analysis of the solutions was performed using MATLAB with the bvp4c. The analysis shows that the first solution is physically feasible and stable in all the graphs. In contrast, the second solution is found to be unstable despite satisfying the initial and boundary conditions of the problem. Therefore, in the present study, only the results of the first solution are discussed, and the results of the second solution are ignored because of their lack of feasibility. To validate the results obtained in this study, they were compared with those obtained previously by Rangi and Ahmad [31], as shown in Table 3. The comparison shows that our results are similar to those reported in the literature. Table 3 shows the numerical values related to the Cu and Fe_3O_4

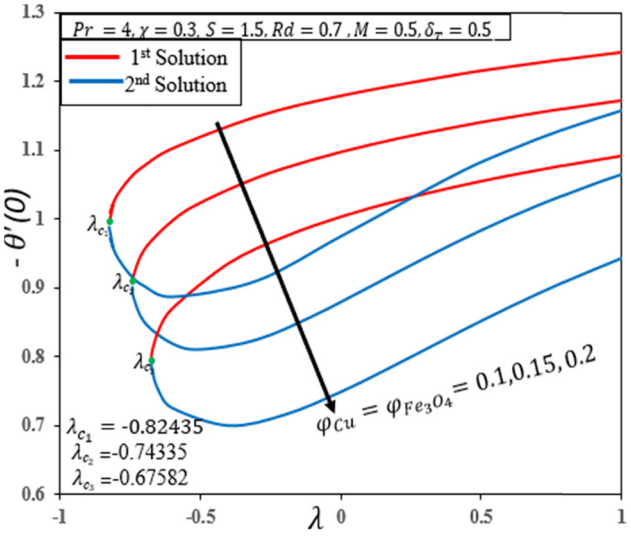

Figure 5: Variations in $\theta'(0)$ along λ for various Fe_3O_4 and Cu nanoparticles.

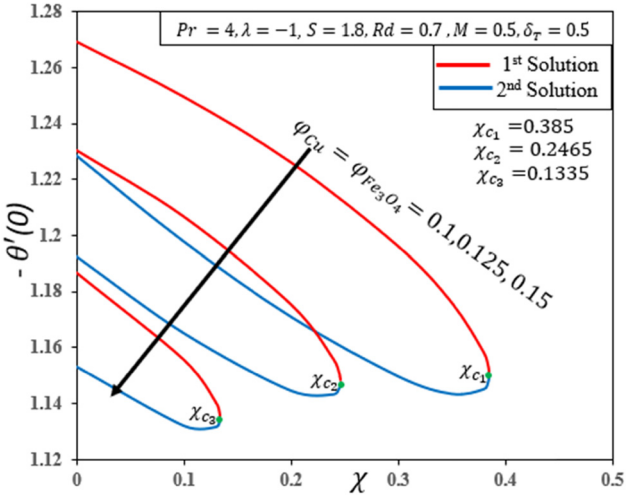

Figure 7: Variations in $\theta'(0)$ along χ for various Fe_3O_4 and Cu nanoparticles.

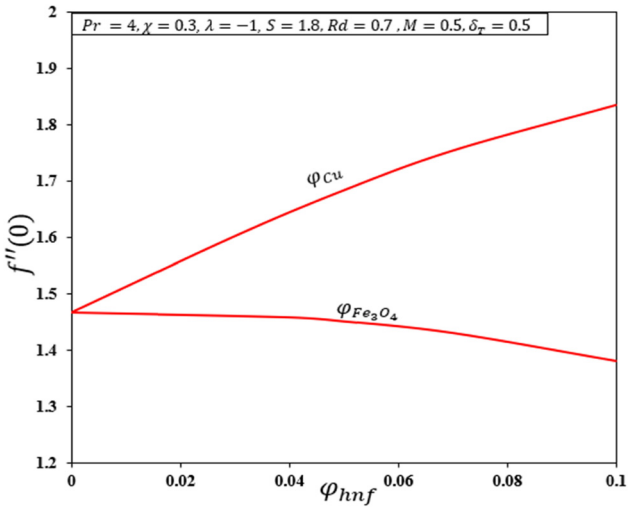

Figure 8: A comparison of the variation in $f''(0)$ for the suspension of Fe_3O_4 and Cu nanoparticles.

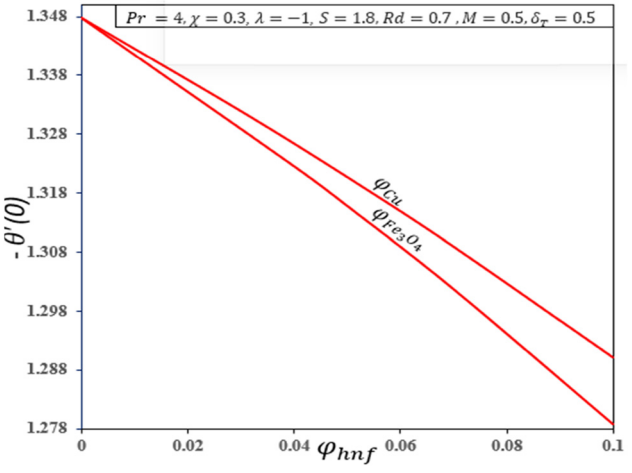

Figure 9: A comparison of the variation in $\theta'(0)$ for the suspension of Fe_3O_4 and Cu nanoparticles.

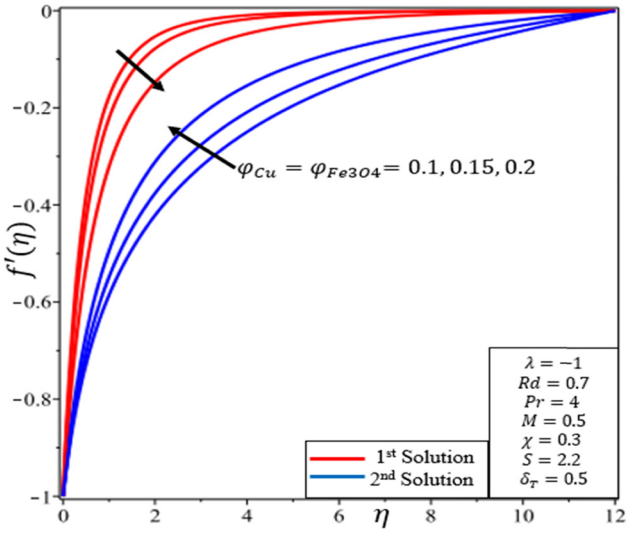

Figure 10: Behavior of φ_{hnf} on $f'(\eta)$.

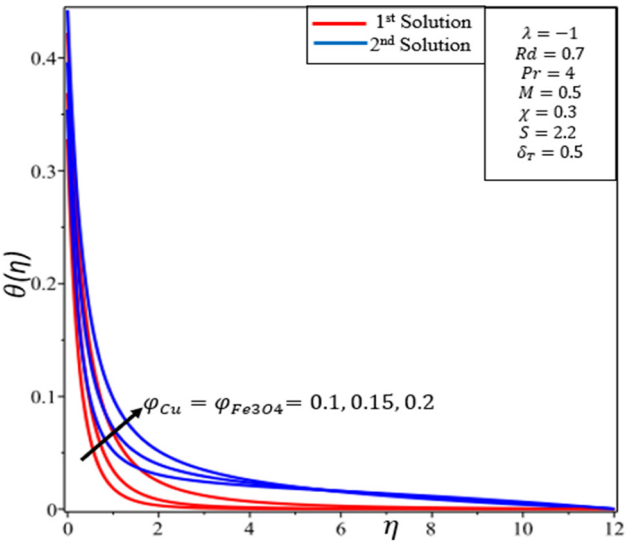

Figure 11: Behavior of φ_{hnf} on $\theta(\eta)$.

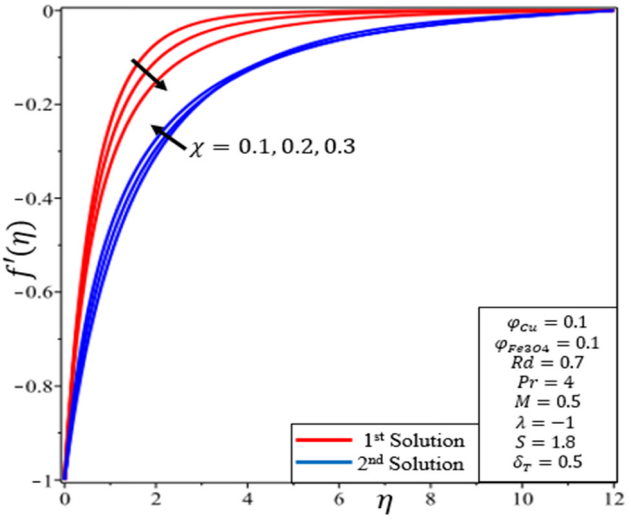

Figure 12: Behavior of χ on $f'(\eta)$.

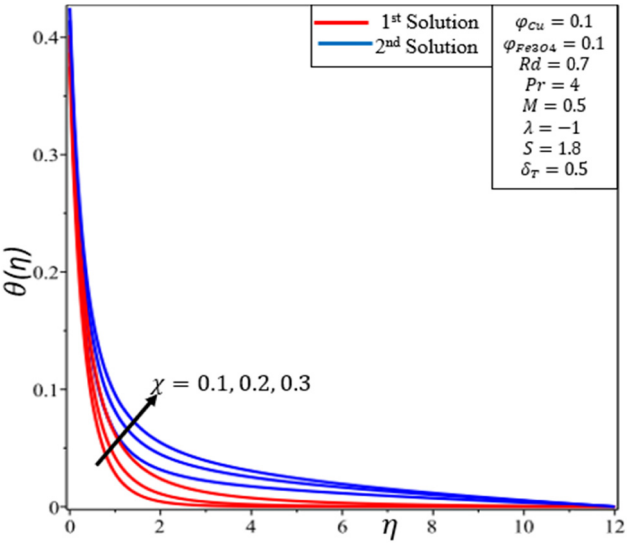

Figure 13: Behavior of χ on $\theta(\eta)$.

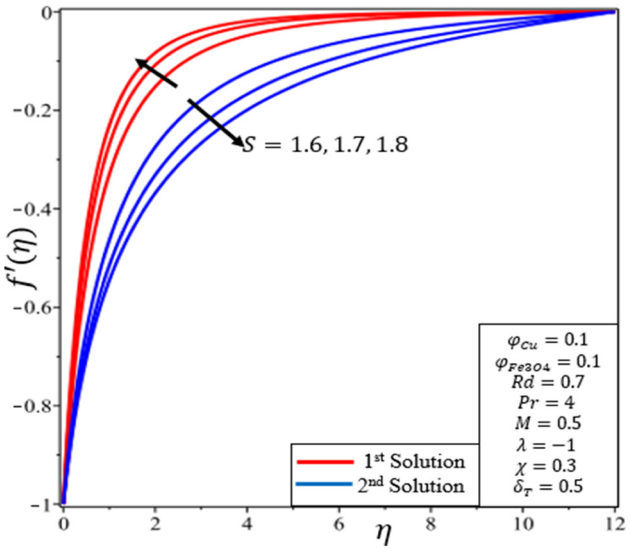

Figure 14: Behavior of S on $f'(\eta)$.

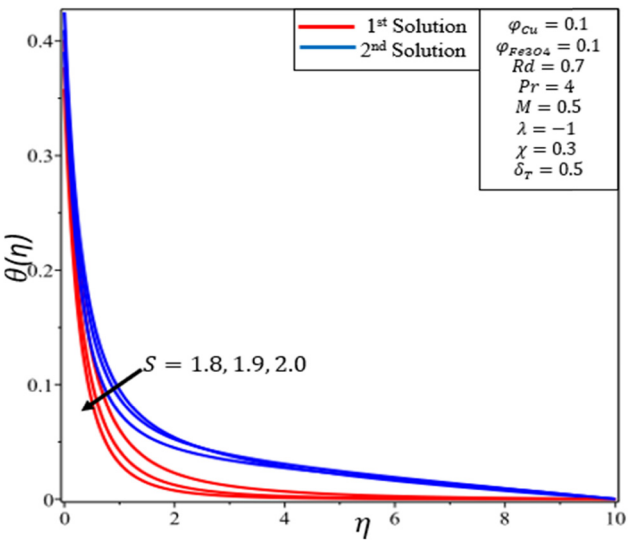

Figure 15: Behavior of S on $\theta(\eta)$.

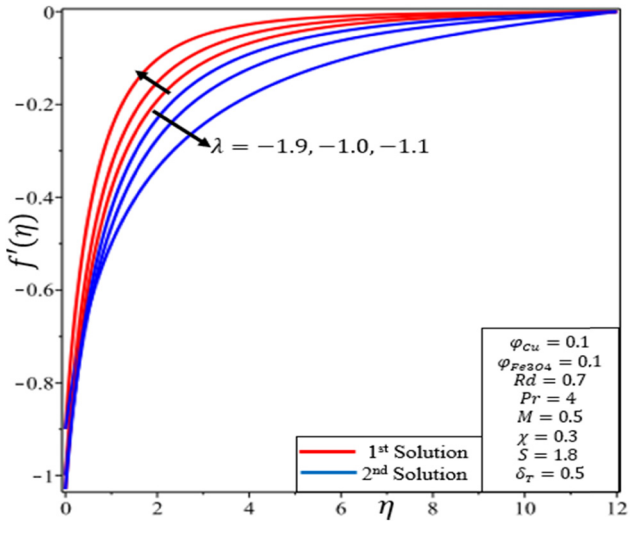

Figure 16: Behavior of λ on $f'(\eta)$.

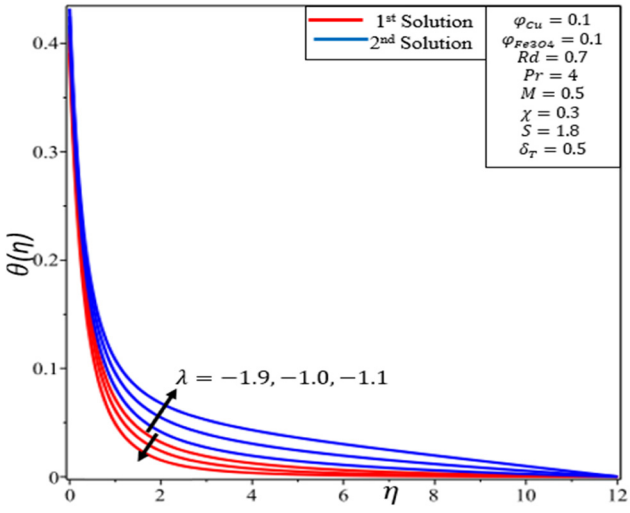

Figure 17: Behavior of λ on $\theta(\eta)$.

nanomaterials as well as the base fluid (blood). Furthermore, in this study, the results of the change in velocity and temperature profiles along the coefficients of skin friction and the Nusselt numbers with variation in values of specified flow parameters and nanoparticle volume fractions are discussed.

Figures 2 and 3 demonstrate the influence of the volume fractions of the used nanoparticles on skin friction and the Nusselt number with respect to the variation in the suction parameter S. At various nanoparticle volume fractions, critical points were obtained where both existing solutions merged into a single common point. The results show that an increase in the nanoparticle volume fraction decreases the drag forces (skin friction) and heat transfer rate (Nusselt number) of blood in stenotic arteries. The nanoparticle volume fraction with changes in the stretching and shrinking parameters λ on skin friction and the Nusselt number are shown in Figures 4 and 5, respectively. The merging points are shown in the graphs. The results illustrate that an increase in the volume fraction of the nanoparticles increases the drag force (skin friction) for $\lambda > 0$ (stretching case) and decreases for $\lambda < 0$ (shrinking case), while the rate of heat transfer (Nusselt number) decreases the blood in the stenotic arteries. Figures 6 and 7 show the influence of the volumetric fraction of nanoparticles on the skin friction and Nusselt number due to the variation in the flow parameter χ.

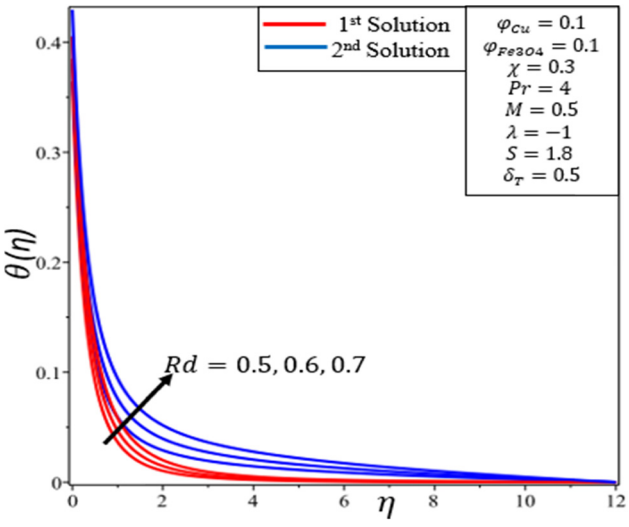

Figure 18: Behavior of Rd on $\theta(\eta)$.

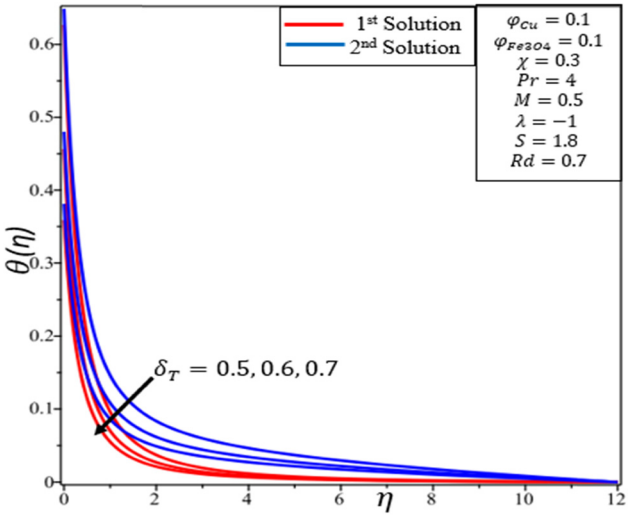

Figure 19: Behavior of δ_T on $\theta(\eta)$.

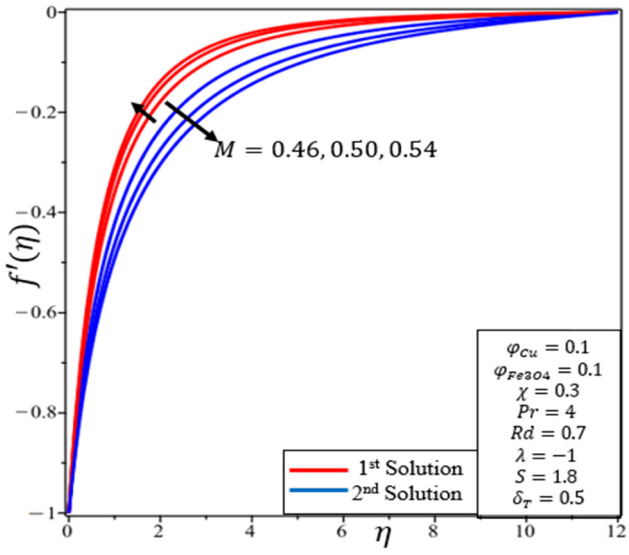

Figure 20: Behavior of M on $f'(\eta)$.

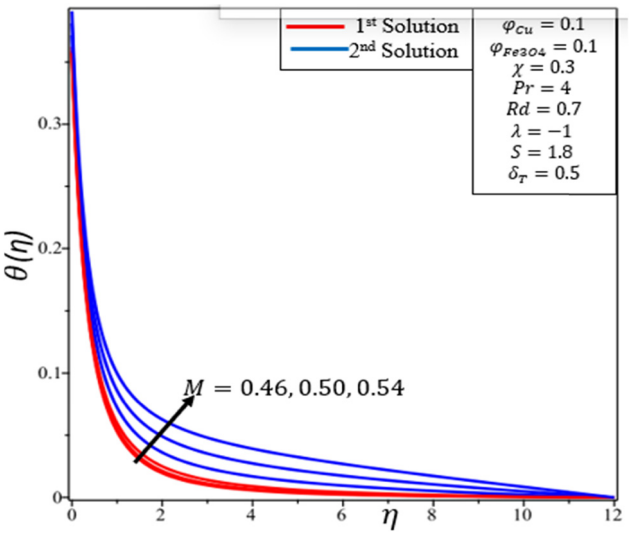

Figure 21: Behavior of M on $\theta(\eta)$.

The findings illustrated that the skin friction and Nusselt number decreased with increasing nanoparticle volume fractions. Figures 8 and 9 illustrate the comparative results of the Cu-blood base nanofluid and Fe_3O_4-blood base nanofluid for the variation in skin friction and local Nusselt number, respectively. The Cu-blood base nanofluid exhibited a greater rate of skin friction and Nusselt number than the Fe_3O_4-blood base nanofluid. Figures 10 and 11 illustrate the significance of the volume fraction of nanoparticles on the velocity and temperature profiles, respectively. The volume fractions of the nanoparticles showed an increase in velocity and temperature profiles of blood through the human stenotic artery when the number of nanoparticles was increased. Figures 12 and 13 show the influence of the flow parameter χ on the velocity and temperature profiles, respectively. The velocity and temperature of the human blood rise with an increment in the flow parameter χ. Figures 14 and 15 illustrate the influence of the suction parameter S on the velocity and temperature profiles, respectively. The results indicate an increase in the rate of suction, a decrease in the velocity, and temperature of human blood during flow through the stenosed artery. Physically, owing to suction, the principle of conservation of mass and energy is affected, which alters the balance of mass and energy, leading to a decrease in the velocity and temperature of the flowing fluid. The effects of

stretching/shrinking parameter λ, velocity, and temperature profiles are illustrated in Figures 16 and 17, respectively. Both the velocity and temperature profiles appeared to decrease with an increase in the rate of shrinking. Figure 18 shows the effect of the radiation parameter Rd on the temperature profile. The temperature of the human blood mixed with copper and iron oxide nanoparticles appears to increase with an increase in the thermal radiation parameter through the stenosed artery. On the other hand, increasing the thermal slip parameter δ_T decreases the temperature of human blood during the flow through a stenosed artery, as shown in Figure 19. Figures 20 and 21 show the influence of the magnetic parameter M on the velocity and temperature profiles, respectively. These figures show that by increasing the magnetic parameter M, the velocity field and temperature of the fluid in the arteries decrease. This is because an increase in the magnetic field develops a Lorentz force, which tends to decrease the blood flow, and due to resistance in the flow, the temperature starts to increase.

5 Conclusion

In the present study, the effects of different flow parameters, i.e., magnetic, suction, thermal radiation, and thermal slip parameters, on the hybrid nanofluid flow along the combined dispersion of Cu and Fe_3O_4 nanoparticles were investigated. Blood is considered the base fluid in this study. The coupled PDEs are converted by using suitable similarity variables to the ODEs to accomplish the requirements of the numerical methodology used, namely, the shooting method, using Maple software. Plasma flow, blood circulation, wire pulling, hot rolling, motor oil transferring, copper deformation, die casting, crystal growth, paper manufacture, engineering, as well as biological science are affected by this problem. The main results of the present study are as follows:

- The specified flow model may improve drug distribution.
- The combined use of Cu and Fe_3O_4 nanomaterials is beneficial for drug transport.
- The solutions (dual) exist only when $S \geq 1.7591$, $\lambda \geq -0.82435$, and $0 \leq \chi \leq 0.7385$.
- The skin friction and Nusselt number decrease with increasing nanoparticle volume fraction along with the variations in suction, stretching/shrinking, and flow parameters.
- By increasing the rate of nanoparticles and the flow parameter, the temperature and flow profiles of blood increase in the arteries.
- The concentration of blood flow can be decreased by increasing the suction, magnetic, and rate of shrinking parameters in the arteries.
- The temperature of the blood can also be improved by increasing the rate of thermal radiation and the magnetic parameters.
- To forecast the cause of atherosclerosis, such modeling and numerical investigations can play an important role.

Acknowledgments: The authors extend their appreciation to the support of Princess Nourah bint Abdulrahman University Researchers Supporting Project number (PNURSP2025R163), Princess Nourah bint Abdulrahman University, Riyadh, Saudi Arabia. In addition, this work is also supported by the Researchers Supporting project (number SHEC/SRSP/N&PS-4/155/2022-23), Sindh Higher Education Commission, Sindh, Pakistan.

Funding information: Princess Nourah bint Abdulrahman University Researchers Supporting Project number (PNURSP2025R163), Princess Nourah bint Abdulrahman University, Riyadh, Saudi Arabia.

Author contributions: S.D. and A.R.N.: conceptualization, methodology, software, formal analysis, validation, and writing – original draft. L.A.L: writing – original draft, data curation, investigation, visualization, and validation. U.K.: conceptualization, writing – original draft, writing – review & editing, supervision, and resources. S.E: validation, investigation, writing – review & editing, formal analysis; project administration; funding acquisition, and software.

Conflict of interest: The authors state no conflict of interest.

Data availability statement: The datasets used and/or analyzed during the current study are available from the corresponding author upon reasonable request.

References

[1] Ellahi, R., S. U. Rahman, and S. Nadeem. Blood flow of Jeffrey fluid in a catheterized tapered artery with the suspension of nanoparticles. *Physics Letters A*, Vol. 378, No. 40, 2014, pp. 2973–2980.

[2] Ijaz, S. and S. Nadeem. Examination of nanoparticles as a drug carrier on blood flow through catheterized composite stenosed artery with permeable walls. *Computer Methods and Programs in Biomedicine*, Vol. 133, 2016, pp. 83–94.

[3] Sarwar, L. and A. Hussain. Flow characteristics of Au-blood nanofluid in stenotic artery. *International Communications in Heat and Mass Transfer*, Vol. 127, 2021, id. 105486.

[4] Abdelsalam, S. I., K. S. Mekheimer, and A. Z. Zaher. Alterations in blood stream by electroosmotic forces of hybrid nanofluid through diseased artery: aneurysmal/stenosed segment. *Chinese Journal of Physics*, Vol. 67, 2020, pp. 314–329.

[5] Shojaie Chahregh, H. and S. Dinarvand. TiO_2-Ag/blood hybrid nanofluid flow through an artery with applications of drug delivery and blood circulation in the respiratory system. *International Journal of Numerical Methods for Heat Fluid Flow*, Vol. 30, No. 11, 2020, pp. 4775–4796.

[6] Shahzadi, I. and S. Bilal. A significant role of permeability on blood flow for hybrid nanofluid through bifurcated stenosed artery: Drug delivery application. *Computer Methods and Programs in Biomedicine*, Vol. 187, 2020, id. 105248.

[7] Dinarvand, S., M. Nademi Rostami, R. Dinarvand, and I. Pop. Improvement of drug delivery micro-circulatory system with a novel pattern of CuO-Cu/blood hybrid nanofluid flow towards a porous stretching sheet. *International Journal of Numerical Methods for Heat Fluid Flow*, Vol. 29, No. 11, 2019, pp. 4408–4429.

[8] Hangaragi, S., N. Neelima, N., Beemkumar, A., Kulshreshta, U., Khan, N. S, Akbar, et al. A computational role of blood nanofluid induced by a stenosed artery with porous medium and thermophoretic particle deposition effects. Alexandria Engineering Journal, Vol. 113, 2025, pp. 32–43.

[9] Zhang, G., J. Luo, M. Sun, Y. Yu, J. Wang, B. Chen, et al. Effect of soft magnetic particles content on multi-physics field of magnetorheological composite gel clutch with complex flow channel excited by Halbach array arrangement. *Composites Part A: Applied Science and Manufacturing*, Vol. 188, 2025, id. 108576.

[10] Saeed, A., A. Alsubie, P. Kumam, S. Nasir, T. Gul, and W. Kumam. Blood-based hybrid nanofluid flow together with electromagnetic field and couple stresses. *Scientific Reports*, Vol. 11, No. 1, 2021, id. 12865.

[11] Kot, M. E. and Y. A. Elmaboud. Hybrid nanofluid flows through a vertical diseased coronary artery with heat transfer. *Journal of Mechanics in Medicine and Biology*, Vol. 21, No. 2, 2021, id. 2150012.

[12] Alhussain, Z. A. and A. Tassaddiq. Thin film blood based Casson hybrid nanofluid flow with variable viscosity. *Arabian Journal for Science and Engineering*, Vol. 47, No. 1, 2022, pp. 1087–1094.

[13] Sajid, T., S. Tanveer, M. Munsab, and Z. Sabir. Impact of oxytactic microorganisms and variable species diffusivity on blood-gold Reiner–Philippoff nanofluid. *Applied Nanoscience*, Vol. 11, No. 1, 2021, pp. 321–333.

[14] Mousavi, S. M., M. N. Rostami, M. Yousefi, and S. Dinarvand. Dual solutions for MHD flow of a water-based TiO_2-Cu hybrid nanofluid over a continuously moving thin needle in presence of thermal radiation. *Reports in Mechanical Engineering*, Vol. 2, No. 1, 2021, pp. 31–40.

[15] Parveen, N., M. Awais, S. Mumraz, A. Ali, and M. Y. Malik. An estimation of pressure rise and heat transfer rate for hybrid nanofluid with endoscopic effects and induced magnetic field: Computational intelligence application. *The European Physical Journal Plus*, Vol. 135, 2020, pp. 1–41.

[16] Choi, S. U. and J. A. Eastman. *Enhancing thermal conductivity of fluids with nanoparticles (No. ANL/MSD/CP-84938; CONF-951135-29)*, Argonne National Lab. (ANL), Argonne, IL (United States), 1995.

[17] Farooq, U., H. Waqas, M. I. Khan, S. U. Khan, Y. M. Chu, and S. Kadry. Thermally radioactive bioconvection flow of Carreau nanofluid with modified Cattaneo-Christov expressions and exponential space-based heat source. *Alexandria Engineering Journal*, Vol. 60, No. 3, 2021, pp. 3073–3086.

[18] Li, Y., H. Waqas, M. Imran, U. Farooq, F. Mallawi, and I. Tlili. A numerical exploration of modified second-grade nanofluid with motile microorganisms, thermal radiation, and Wu's slip. *Symmetry*, Vol. 12, No. 3, 2020, id. 393.

[19] Motasadizadeh, H., M. Tavakoli, S. Damoogh, F. Mottaghitalab, M. Gholami, F. Atyabi, et al. Dual drug delivery system of teicoplanin and phenamil based on pH-sensitive silk fibroin/sodium alginate hydrogel scaffold for treating chronic bone infection. *Biomaterials Advances*, Vol. 139, 2022, id. 213032.

[20] Sabzi, M., S. M. Far, and S. M. Dezfuli. Characterization of bioactivity behavior and corrosion responses of hydroxyapatite-ZnO nanostructured coating deposited on NiTi shape memory alloy. *Ceramics International*, Vol. 44, No. 17, 2018, pp. 21395–21405.

[21] Hajipour, P., A. Eslami, A. Bahrami, A. Hosseini-Abari, F. Y. Saber, R. Mohammadi, et al. Surface modification of TiO_2 nanoparticles with CuO for visible-light antibacterial applications and photocatalytic degradation of antibiotics. *Ceramics International*, Vol. 47, No. 23, 2021, pp. 33875–33885.

[22] Shen, B., S. Xiao, C. Yu, C. Zhang, J. Zhan, Y. Liu, et al. Cerebral hemodynamics underlying ankle force sense modulated by high-definition transcranial direct current stimulation. *Cerebral Cortex*, Vol. 34, No. 6, 2024, id. bhae226.

[23] Zeng, W., P. Zhou, Y. Wu, D. Wu, and M. Xu. Multi-cavitation states diagnosis of the vortex pump using a combined DT-CWT-VMD and BO-LW-KNN based on motor current signals. *IEEE Sensors Journal*, Vol. 24, No. 19, 2024, pp. 30690–30705.

[24] He, J., Q. Hou, X. Yang, H. Duan, and L. Lin. Isolated slug traveling in a voided line and impacting at an end orifice. *Physics of Fluids*, Vol. 36, No. 2, 2024.

[25] Wu, C., J. Deng, X. Zhou, A. Gao, K. Feng, and C. Zhu. Turbulence affected by submerged aquatic vegetation under wind-induced flow. *Physics of Fluids*, Vol. 37, No. 1, 2025.

[26] Mao, Z., N. Hosoya, and S. Maeda. Flexible electrohydrodynamic fluid-driven valveless water pump via immiscible interface. *Cyborg and Bionic Systems*, Vol. 5, 2024, id. 0091.

[27] Sarwar, L., A. Hussain, U. Fernandez-Gamiz, S. Akbar, A. Rehman, and E. S. Sherif. Thermal enhancement and numerical solution of blood nanofluid flow through stenotic artery. *Scientific Reports*, Vol. 12, No. 1, 2022, id. 17419.

[28] Sharma, B. K., R. Gandhi, T. Abbas, and M. M. Bhatti. Magnetohydrodynamics hemodynamics hybrid nanofluid flow through inclined stenotic artery. *Applied Mathematics and Mechanics*, Vol. 44, No. 3, 2023, pp. 459–476.

[29] Harris, S. D., D. B. Ingham, and I. Pop. Mixed convection boundary-layer flow near the stagnation point on a vertical surface in a porous medium: Brinkman model with slip. *Transport in Porous Media*, Vol. 77, 2009, pp. 267–285.

[30] Mutuku-Njane, W. N. *Analysis of hydromagnetic boundary layer flow and heat transfer of nanofluids*. PhD diss., Cape Peninsula University of Technology, 2014.

[31] Rangi, R. R. and N. Ahmad. Boundary layer flow past a stretching cylinder and heat transfer with variable thermal conductivity. *Applied Mathematics*, Vol. 3, No. 3, 2012, pp. 205–209.